Polarizing electron spins with a superconducting flux qubit

Shingo Kukita,[1,*] Hideaki Ookane,[1,†] Yuichiro Matsuzaki,[2,‡] and Yasushi Kondo[1,§]
[1]*Department of Physics, Kindai University, Higashi-Osaka 577-8502, Japan*
[2]*Device Technology Research Institute, National Institute of Advanced Industrial Science and Technology (AIST), 1-1-1, Umezono, Tsukuba, Ibaraki 305-8568, Japan*

(Received 6 August 2021; revised 4 November 2021; accepted 3 January 2022; published 28 January 2022)

Electron-spin resonance is a useful tool to investigate properties of materials in magnetic fields where high spin polarization of target electron spins is required in order to obtain high sensitivity. However, the smaller the magnetic fields becomes, the more difficult it is to obtain high polarization by thermalization. Here, we propose to employ a superconducting flux qubit (FQ) to polarize electron spins actively. We have to overcome a large energy difference between the FQ and electron spins for efficient energy transfer among them. For this purpose, we adopt a spin-lock technique on the FQ where the Rabi frequency associated with the spin-locking can match the resonance (Larmor) one of the electron spins. We find that adding dephasing on the spins is beneficial to obtain high polarization of them, because otherwise the electron spins are trapped in dark states that cannot be coupled with the FQ. We show that our scheme can achieve high polarization of electron spins in realistic experimental conditions.

DOI: 10.1103/PhysRevA.105.012613

I. INTRODUCTION

Increasing attention has been paid to electron-spin resonance (ESR) due to an excellent sensitivity compared with that of nuclear magnetic resonance (NMR). An improvement of the ESR sensitivity is important for practical applications. Therefore, superconducting circuits have often been used to detect a small number of electron spins [1–8]. By using a superconducting resonator, it is possible to measure only 12 spins with 1 s measurement time where the detection volume is around 6 fL [9] where the frequency of the superconducting resonator is fixed. It is favorable to sweep not only the microwave frequency but also the magnetic field to investigate complicated spin systems. For this purpose, we could use a waveguide [10], a frequency tunable resonator [11], or a direct current-superconducting quantum interference device (dcSQUID) [2,12]. Among these approaches, a superconducting flux qubit (FQ) is promising and has already achieved a sensitivity of 20 spins/$\mathrm{Hz}^{1/2}$ with a sensing volume of 6 fL for the ESR [13].

It is worth mentioning that the FQ cannot work if we apply high magnetic fields, so the applied field should be smaller than 10 mT [2]. One of the problems in FQ-ESR measurements is a low polarization of target electrons, especially when they are in a low magnetic field. A typical thermal energy $\approx k_{\mathrm{B}}T$ (k_{B} is the Boltzmann constant and T is the temperature) at mK temperatures is around hundreds of MHz in frequency units, while the typical magnetic energy of the electron spins $\approx \mu_{\mathrm{B}}B$ (μ_{B} is the Bohr magneton constant and B is flux density in tesla) in a small field of few mT is about tens of MHz. This implies that the electron spins cannot be fully polarized in these conditions and that the sensitivity of ESR is deteriorated. Note that high spin polarization of target electrons is required in order to obtain high sensitivity [14]. A Purcell effect [15] was recently employed to polarize electron spins with a superconducting cavity [16]. However, this is not applicable to the case when electron spins are placed in a low magnetic field because of a large energy difference between the cavity and electron spins. Moreover, a thermal relaxation time of electron spins becomes larger at lower temperature, and thus it is difficult to polarize them [17–20].

Here, we propose to employ a FQ for not only detecting but also polarizing electron spins. The main idea is that the energy relaxation time of the FQ is much shorter than that of the electron spins, and so we can efficiently emit the energy of the electron spin to the environment by using a coupling between the FQ and electron spins. We adopt a spin-lock technique where the Rabi frequency of the FQ in a rotating frame associated with the spin-locking matches with the resonance (Larmor) frequency of the electron spins in a low magnetic field [21]. The important difference from the polarization with a Purcell effect [16] is that the Rabi frequency can be much smaller than the resonance one of the FQ. By using a long-lived FQ such as a capacitively shunted FQ whose coherence time is around tens of microseconds [22–24], the Rabi frequency can be reduced to hundreds of kHz. With these properties, one may overcome the energy scale mismatch between a FQ and electron spins, and thus the efficient polarization of the electron spins becomes possible.

This paper is organized as follows: Section II illustrates our setup and proposal with analytical discussion on a simplified model. We show our numerical simulations with realistic

*toranojoh@phys.kindai.ac.jp
†h-okane@phys.kindai.ac.jp
‡matsuzaki.yuichiro@aist.go.jp
§ykondo@kindai.ac.jp

experimental parameters in Sec. III for demonstrating its experiment feasibility. We conclude this paper in Sec. IV.

II. THEORY

We here propose to employ a Hartmann-Hahn (H-H) resonance [21] to polarize electron spins with a FQ. The H-H resonance has been applied to polarize environmental spins by using nitrogen vacancy (NV) centers in diamond [25,26]. Our proposal is expected to polarize far more electron spins than the case of the NV center in diamond because the size of the FQ is of the order of micrometers while that of the NV center is of the order of angstroms.

We discuss a simplified model in order to illustrate our proposal after introducing a Hamiltonian and Lindbladian that govern the electron spins and FQ.

A. Model

The Hamiltonian of a FQ coupled to M electron spins (labeled with $k = 1$–M) is described as follows:

$$H = H_{\rm FQ} + H_{\rm spin} + H_{\rm I},$$

where $H_{\rm FQ}$, $H_{\rm spin}$, and $H_{\rm I}$ denote the Hamiltonian of the FQ, spins, and interaction between them. $H_{\rm FQ}$ is given as

$$H_{\rm FQ} = \frac{\Delta}{2}Z + \frac{\epsilon}{2}X + \lambda X\cos\omega t,$$

where ϵ denotes the energy bias, Δ the tunneling energy, ω the frequency of the microwave, and λ the strength of the microwave. X, Y, and Z are standard Pauli matrices acting on the FQ. It is convenient for us to change the notation, and we rewrite $H_{\rm FQ}$ as follows:

$$H_{\rm FQ} = \frac{\Delta}{2}\sigma_x^{(0)} + \frac{\epsilon}{2}\sigma_z^{(0)} + \lambda\sigma_z^{(0)}\cos\omega t,$$

where we change X and Z to $\sigma_z^{(0)}$ and $\sigma_x^{(0)}$. Hereafter, we identify the 0th degree of freedom, which is represented by the superscript 0, with the flux qubit (FQ), and the other degrees of freedom ($k = 1$–M) with the electron spins. $H_{\rm spin}$ and $H_{\rm I}$ are given as

$$H_{\rm spin} = \sum_{k=1}^{M}\frac{\omega_k}{2}\sigma_z^{(k)},$$

$$H_{\rm I} = \sum_{k=1}^{M} g_k\sigma_z^{(0)}\sigma_x^{(k)},$$

where $\frac{\omega_k}{2}$ denotes the resonance frequency of the kth spin and g_k the coupling strength between the FQ and the kth spin.

We rewrite the Hamiltonian by using the basis to diagonalize $\frac{\Delta}{2}\sigma_x^{(0)} + \frac{\epsilon}{2}\sigma_z^{(0)}$ as follows:

$$H = \frac{\sqrt{\epsilon^2+\Delta^2}}{2}\sigma_z^{(0)} + \lambda\frac{\Delta}{\sqrt{\epsilon^2+\Delta^2}}\sigma_x^{(0)}\cos\omega t + \lambda\frac{\epsilon}{\sqrt{\epsilon^2+\Delta^2}}\sigma_z^{(0)}\cos\omega t + \sum_{k=1}^{M}\frac{\omega_k}{2}\sigma_z^{(k)} + \sum_{k=1}^{M} g_k\frac{\epsilon}{\sqrt{\epsilon^2+\Delta^2}}\sigma_z^{(0)}\sigma_x^{(k)} + \sum_{k=1}^{M} g_k\frac{\Delta}{\sqrt{\epsilon^2+\Delta^2}}\sigma_x^{(0)}\sigma_x^{(k)}.$$

By going to a rotating frame with a frequency of $\omega = (\epsilon^2+\Delta^2)^{1/2}$ of the FQ, we obtain the following Hamiltonian with a rotating wave approximation:

$$H \simeq \frac{\lambda}{2}\frac{\Delta}{\sqrt{\epsilon^2+\Delta^2}}\sigma_x^{(0)} + \sum_{k=1}^{M}\frac{\omega_k}{2}\sigma_z^{(k)} + \sum_{k=1}^{M} g_k\frac{\epsilon}{\sqrt{\epsilon^2+\Delta^2}}\sigma_z^{(0)}\sigma_x^{(k)}.$$

We change the notation from $\sigma_x^{(0)}$ ($\sigma_z^{(0)}$) to $\sigma_z^{(0)}$ ($\sigma_x^{(0)}$), and the Hamiltonian is rewritten as

$$H \simeq \frac{\lambda}{2}\frac{\Delta}{\sqrt{\epsilon^2+\Delta^2}}\sigma_z^{(0)} + \sum_{k=1}^{M}\frac{\omega_k}{2}\sigma_z^{(k)} + \sum_{k=1}^{M} g_k\frac{\epsilon}{\sqrt{\epsilon^2+\Delta^2}}\sigma_x^{(0)}\sigma_x^{(k)}.$$

We obtain the following effective Hamiltonian in a rotating frame of which the frequency is $\omega_{\rm avg} = \frac{1}{M}\sum_k\omega_k$ with the rotating wave approximation:

$$H \simeq \sum_{k=1}^{M}\left[\frac{\omega_k'}{2}\sigma_z^{(k)} + g_k\frac{\epsilon}{\sqrt{\epsilon^2+\Delta^2}}(\sigma_+^{(0)}\sigma_-^{(k)} + \sigma_-^{(0)}\sigma_+^{(k)})\right], \tag{1}$$

where $\omega_k' = \omega_k - \omega_{\rm avg}$ and $\sigma_\pm = \sigma_x \pm i\sigma_y$. Here, we set $\lambda\frac{\Delta}{(\epsilon^2+\Delta^2)^{1/2}}$ to be $\omega_{\rm avg}$. It is worth mentioning that the Rabi frequency λ can be as large as $2\pi \times 1.7$ GHz for the flux qubit [27].

The energy exchanges occur between the FQ and electron spins during the irradiation of a microwave due to the above flip-flop interaction, while there is no coupling between them in the absence of the irradiation due to the energy detuning of $(\epsilon^2+\Delta^2)^{1/2} \gg \omega_k/2$.

We also introduce the Lindblad operator in order to describe the relaxation of the system (= a FQ and spins), as follows:

$$\mathcal{L}[\rho] = \sum_{l=0}^{M}\gamma_{\rm T}^{(l)}\left(\sigma_z^{(l)}\rho\sigma_z^{(l)} - \rho\right) + \sum_{l=0}^{M}\gamma_{\rm L}^{(l)}(\sigma_+^{(l)}\rho\sigma_-^{(l)} + \sigma_-^{(l)}\rho\sigma_+^{(l)} - \rho), \tag{2}$$

where $\gamma_{\rm T}$ and $\gamma_{\rm L}$ characterize the strengths of transversal and longitudinal relaxations, respectively. Note that the superscript l runs from 0 to M while k runs from 1 to M. We consider the case when each qubit (FQ or spins) has a different relaxation parameter labeled with $*^{(l)}$.

A system dynamics is then determined by

$$\frac{d\rho}{dt} = -i[H, \rho] + \mathcal{L}[\rho], \tag{3}$$

while the initial state is assumed to be

$$\rho(0) = |0\rangle\langle 0| \otimes \bigotimes_{k=1}^{M} \frac{\sigma_0}{2}, \tag{4}$$

where σ_0 is the 2×2 identity matrix. Then, our goal is to obtain

$$\rho(\text{final}) = |0\rangle\langle 0| \otimes \bigotimes_{k=1}^{M} |0\rangle\langle 0|, \tag{5}$$

after some operations.

B. Simplified model

We consider a simplified model where ω_k and g_k are identical for $k = 1$–M. Due to this simplification, we can calculate polarization dynamics for a large number of spins. Our procedure consists of two steps, Steps I and II. A FQ interacts with the spins and absorbs their entropy in Step I while the spin states are homogenized with a help of dephasing in Step II.

(i) in Step I

Let the system develop according to the following simplified Hamiltonian: This is obtained from Eq. (1) by assuming $g_k = g$ and $\omega_k' = 0$ for $k = 1$–M,

$$H^{\mathrm{I}} = g(\sigma_+^{(0)} S_- + \sigma_-^{(0)} S_+),$$
$$S_{x,y,z,\pm} = \sum_{k=1}^{M} \sigma_{x,y,z,\pm}^{(k)}, \tag{6}$$

while the Lindbladian (2) is simplified as

$$\mathcal{L}^{\mathrm{I}}[\rho] = \gamma\left(\sigma_z^{(0)} \rho \sigma_z^{(0)} - \rho\right), \tag{7}$$

where we assume that only $\gamma_{\mathrm{T}}^{(0)} = \gamma \neq 0$ and the other $\gamma_{\mathrm{T}}^{(k)}$ and $\gamma_{\mathrm{L}}^{(l)}$ are negligible. The only FQ is under influence of dephasing.

After the dynamics, we initialize the FQ to the ground state $|0\rangle$ without disturbing the spins ($k = 1$–M).

(ii) in Step II

We decouple the FQ from the spins. Therefore, the Hamiltonian is given as

$$H^{\mathrm{II}} = 0, \tag{8}$$

while the Lindbladian (2) in Step II is simplified as

$$\mathcal{L}^{\mathrm{II}}[\rho] = \sum_{k=1}^{M} \gamma'\left(\sigma_z^{(k)} \rho \sigma_z^{(k)} - \rho\right), \tag{9}$$

where we assume that only $\gamma_{\mathrm{T}}^{(k)} = \gamma' \neq 0$ and the other $\gamma_{\mathrm{T}}^{(0)}$ and $\gamma_{\mathrm{L}}^{(l)}$ are negligible. All spins are under influence of the same dephasing.

C. Step I

We employ the Young-Yamanouchi basis $|j, m, i\rangle$ [28] in order to represent the spin state. Note that $j = 1/2, 3/2, \ldots, M/2$ and $|m| \leqslant j$ (half-integer) for odd-M cases while $j = 0, 1, \ldots, M/2$ and $|m| \leqslant j$ (integer) for the even-M cases. The index i represents the number of ways of composing n spins to obtain the total angular momentum j and takes 1–d_j, where $d_j := (2j+1)M!/(M/2+j+1)!(M/2-j)!$. The action of spin operators $S_{\pm,z}$ is given as follows:

$$S_+|j, m, i\rangle = \sqrt{j(j+1) - m(m+1)}\,|j, m+1, i\rangle,$$
$$S_-|j, m, i\rangle = \sqrt{j(j+1) - m(m-1)}\,|j, m-1, i\rangle,$$
$$\frac{S_z}{2}|j, m, i\rangle = m|j, m, i\rangle. \tag{10}$$

Let us define

$$|a_{jmi}\rangle := |0\rangle \otimes |j, m, i\rangle, |b_{jmi}\rangle := |1\rangle \otimes |j, m-1, i\rangle. \tag{11}$$

By using the above bases, the initial state (4) can be rewritten as

$$\rho(0) = \frac{1}{2^M} \sum_{j,m,i} |a_{jmi}\rangle\langle a_{jmi}|. \tag{12}$$

The dynamics of $\rho(t)$ from the above initial state according to Eq. (3) with Eqs. (6) and (7) is easily obtained with the help of Eqs. (10–12):

$$\rho(t) = \frac{1}{2^M} \sum_{j,m,i} \rho_{jmi}(t),$$
$$\rho_{jmi}(t) := a_{jmi}(t)|a_{jmi}\rangle\langle a_{jmi}| + b_{jmi}(t)|b_{jmi}\rangle\langle b_{jmi}| + c_{jmi}(t)|a_{jmi}\rangle\langle b_{jmi}| + c_{jmi}^*(t)|b_{jmi}\rangle\langle a_{jmi}|. \tag{13}$$

Here the coefficients $a_{jmi}(t)$, $b_{jmi}(t)$, $c_{jmi}(t)$ satisfy the following differential equations:

$$\dot{a}_{jmi}(t) = -2g l_{jm} c_{jmi}^I(t),$$
$$\dot{b}_{jmi}(t) = 2g l_{jm} c_{jmi}^I(t),$$
$$\dot{c}_{jmi}^I(t) = g l_{jm} a_{jmi}(t) - g l_{jm} b_{jmi}(t) - 2\gamma c_{jmi}^I(t),$$
$$\dot{c}_{jmi}^R(t) = -2\gamma c_{jmi}^R(t), \tag{14}$$

where $c_{jmi}^{I\,(R)}(t)$ is the imaginary (real) part of c_{jmi} and $l_{jm} = \sqrt{j(j+1) - m(m-1)}$. The dynamics of each $\rho_{jmi}(t)$, or the dynamics of $\{a_{jmi}(t), b_{jmi}(t), c_{jmi}(t)\}$, is independent of the other.

Let us now focus on the dynamics of $\rho_{jmi}(t)$ for fixed j, m, i. Because the dynamics of $c_{jmi}^R(t)$ is decoupled from those of the other variables, we assume that c_{jmi} is pure imaginary from now on. The eigenvalues of this dynamics (= decay rates) are given as

$$0, \quad \frac{-\gamma + \sqrt{\gamma^2 - (16 g l_{jm})^2}}{2}, \quad \frac{-\gamma - \sqrt{\gamma^2 - (16 g l_{jm})^2}}{2}. \tag{15}$$

The eigenstate corresponding to the eigenvalue 0 is $\frac{1}{2}|a_{jmi}\rangle\langle a_{jmi}| + \frac{1}{2}|b_{jmi}\rangle\langle b_{jmi}|$ and is independent of γ. Note that this state corresponds to the fully mixed state in the space spanned by $|a_{jmi}\rangle$ and $|b_{jmi}\rangle$ and is stationary.

Let us consider the dynamics of which initial state is given as

$$\rho = \sum_{j,m,i} p_{j,m} |a_{jmi}\rangle\langle a_{jmi}|. \tag{16}$$

The states at the beginning and the end of Steps I + II (and also the initial state) can be always written in the above form, as shown below. The reason why $p_{j,m}$ is independent of the index i is that there is no way to control the freedom of i in our protocol and the initial state is also set to be independent of the index i. Because the dynamics of each $|a_{jmi}\rangle\langle a_{jmi}|$ is independent of each other, the dynamics from the initial state (16) is simply given as

$$\rho(t) = \sum_{j,m,i} p_{j,m} \rho_{jmi}(t). \tag{17}$$

Then, it is assumed that we can wait until the above dynamics converges. After that, we obtain the stationary state of which density matrix $\rho_{\rm st}$ is given as

$$\rho_{\rm st} = \sum_{j,m,i} \frac{p_{j,m}}{2} (|a_{jmi}\rangle\langle a_{jmi}| + |b_{jmi}\rangle\langle b_{jmi}|). \tag{18}$$

We then cut the interaction between the FQ and the spins and initialize the FQ state to the ground state $|0\rangle$. The final total density matrix is given as

$$\rho^{\rm I} = |0\rangle\langle 0| \otimes {\rm Tr}_0(\rho_{\rm st}) = \sum_{j,m,i} p'_{j,m} |a_{jmi}\rangle\langle a_{jmi}|, \tag{19}$$

where ${\rm Tr}_0$ denotes that only the FQ degrees of freedom is traced out. By simple calculations, we obtain

$$\begin{aligned} p'_{j,j} &= \frac{p_{j,j}}{2}, \\ p'_{j,m} &= \frac{p_{j,m}}{2} + \frac{p_{j,m+1}}{2}, \quad m \neq j, -j \\ p'_{j,-j} &= p_{j,-j} + \frac{p_{j,-j+1}}{2}. \end{aligned} \tag{20}$$

Thus, the repetition of Step I can be completely represented by the above update rule (20). See Fig. 1.

The above processes (dynamics + trace out + initialization) is called Step I hereinafter. Figure 2 shows the global view of the whole density-matrix dynamics during Step I.

D. Step II

Even when we repeat the Step I, we cannot polarize all spins, because of the existence of the so-called dark states of $|j, -j, i\rangle$ [29–36]. By the repetitive application of Step I, the population of each basis $|a_{jmi}\rangle\langle a_{jmi}|$ in Eq. (16) except that of the dark states converges to zero and thus the populations will be accumulated onto these dark states. At the infinite-repetition limit, the density matrix is given as

$$\rho = \sum_{j,m,i} \delta_{m,-j} p^{\infty}_{j,-j} |a_{jmi}\rangle\langle a_{jmi}|, \quad p^{\infty}_{j,-j} := \frac{2j+1}{2^M}. \tag{21}$$

Therefore, we cannot achieve perfect polarization only by Step I.

To overcome this problem, in Step II, we apply dephasing noise to the spins ($k = 1$–M) of which state is given by $\rho^{\rm I}$

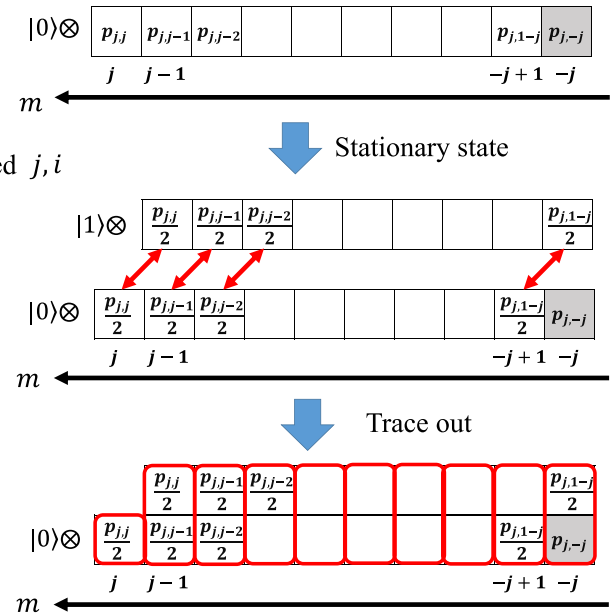

FIG. 1. Schematic picture of dynamics of Step I which consists of "obtaining stationary state, $\rho \to \rho_{\rm st}$" and "trace out" processes. In the $\rho \to \rho_{\rm st}$ process, we have initially $\rho = \sum_{j,m,i} p_{j,m} |a_{jmi}\rangle\langle a_{jmi}|$ where $|a_{jmi}\rangle = |0\rangle \otimes |j, m, i\rangle$, which is illustrated in the upper row. When the system becomes stationary state, we obtain $\rho_{\rm st} = \sum_{j,m,i} \frac{p_{j,m}}{2} (|a_{jmi}\rangle\langle a_{jmi}| + |b_{jmi}\rangle\langle b_{jmi}|)$ where $|b_{jmi}\rangle = |1\rangle \otimes |j, m-1, i\rangle$, and we intuitively show this in the middle row. When the FQ is isolated from the spins and initialized at the end of Step I, we obtain $\rho^{\rm I} = \sum_{j,m,i} p'_{j,m} |a_{jmi}\rangle\langle a_{jmi}|$, as shown in the bottom row. The gray zones represent the dark state.

[Eq. (19)] according to Eq. (9), and we wait until the dynamics converges. We will prove that the density matrix after Step II is given as

$$\rho^{\rm II} = \sum_{j,m,i} P_m |a_{jmi}\rangle\langle a_{jmi}|. \tag{22}$$

The dephasing removes the j dependence in the probability of $|a_{jmi}\rangle\langle a_{jmi}|$. Note that the density matrix given in Eq. (22) is also a special case of Eq. (16).

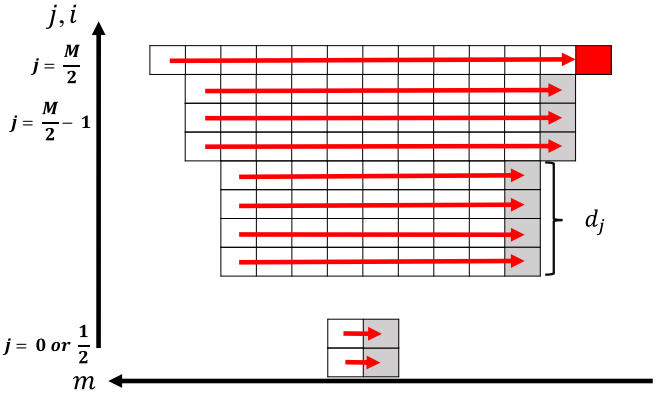

FIG. 2. Global view of the repetitive application of the update rule (20) of Step I. The states of $|j, m, i\rangle$ converges to the states of $|j, -j, i\rangle$. The red zone represents the target polarized state where every spin is in the ground state.

We first introduce $\rho_{j,m}$ which is given as

$$\rho_{j,m} := \sum_{i=1}^{d_j} |a_{jmi}\rangle\langle a_{jmi}|. \tag{23}$$

Let us denote the operation of Step II by $\mathcal{E}_{\rm II}$. Then the dynamics of Step II is given as

$$\rho^{\rm II} = \mathcal{E}_{\rm II}(\rho_{\rm I}) = \sum_{j,m} p'_{j,m}[\mathcal{E}_{\rm II}(\rho_{j,m})]. \tag{24}$$

The action of $\mathcal{E}_{\rm II}$ is written as

$$\mathcal{E}_{\rm II}(\rho_{j,m}) = \frac{d_j}{{}_M C_{m+M/2}} \sum_{s=|m|}^{M/2} \sum_{i=1}^{d_s} |a_{smi}\rangle\langle a_{smi}|, \tag{25}$$

which is shown in Appendix A. After showing the $\sum$ in $\rho^{\rm I}$ explicitly, we transform $\rho^{\rm I}$ as follows:

$$\begin{aligned}
\rho^{\rm II} &= \sum_{m=-M/2}^{M/2} \sum_{j=|m|}^{M/2} p'_{j,m} \left(\frac{d_j}{{}_M C_{m+M/2}} \sum_{s=|m|}^{M/2} \sum_{i=1}^{d_s} |a_{smi}\rangle\langle a_{smi}| \right) \\
&= \sum_{m=-M/2}^{M/2} \left(\sum_{j=|m|}^{M/2} p'_{j,m} \frac{d_j}{{}_M C_{m+M/2}} \right) \sum_{s=|m|}^{M/2} \sum_{i=1}^{d_s} |a_{smi}\rangle\langle a_{smi}| \\
&= \sum_{m=-M/2}^{M/2} P_m \sum_{s=|m|}^{M/2} \sum_{i=1}^{d_s} |a_{smi}\rangle\langle a_{smi}| \\
&= \sum_{j,m,i} P_m |a_{jmi}\rangle\langle a_{jmi}|,
\end{aligned} \tag{26}$$

where P_m is given as

$$\begin{aligned}
P_m &= \sum_{j=|m|}^{M/2} p'_{j,m} \frac{d_j}{{}_M C_{m+\frac{M}{2}}} \\
&= \frac{1}{{}_M C_{m+\frac{M}{2}}} \sum_{j=|m|}^{M/2} \sum_{i=1}^{d_j} p'_{j,m}.
\end{aligned} \tag{27}$$

Because the number of orthogonal states $|a_{jmi}\rangle$ for each m is ${}_M C_{m+\frac{M}{2}}$, this process can be considered as an averaging process of $p'_{j,m}$ in $\rho^{\rm I}$ for a fixed m. (See Fig. 3 for an intuitive explanation of Step II.) Thus, Step II can be totally represented by the update rule,

$$p'_{j,m} \to P_m. \tag{28}$$

Figure 4 shows the schematic view of the whole density-matrix dynamics after Step II.

E. Step I + Step II

It is possible to polarize the spins to ground states by combining Steps I and II. To consider the polarization process, it is convenient to employ the following variable:

$$\Pi_m = \sum_{j=|m|}^{M/2} \sum_{i=1}^{d_j} p_{j,m}, \tag{29}$$

which is the total probability of the mth column states, see Fig. 5. These states have the same energy. If $p_{j,m} = P_m$ (after Step II and the initial state), this is given as

$$\Pi_m = {}_M C_{m+\frac{M}{2}} P_m. \tag{30}$$

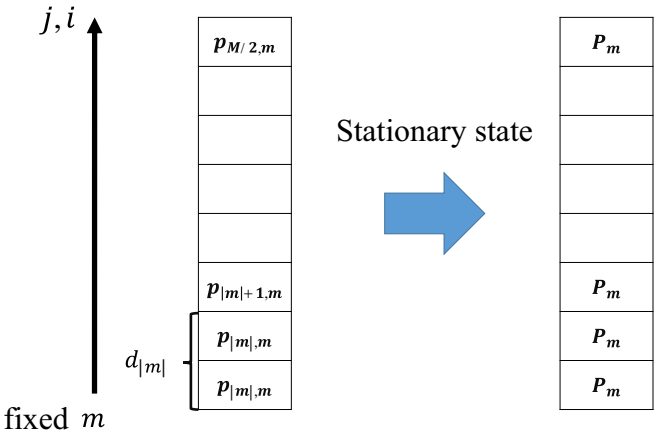

FIG. 3. Step II can be regarded as a process of averaging of $p_{j,m}$ about j and i for fixed m. After Step II, the population of $|j, m, i\rangle$ in the density matrix does not depend on j.

We now consider the update rule of Π_m under Steps I and II. Let us denote the total probability of the mth column states after the nth repetition by $\Pi_m^{(n)}$. The update rule depends on the sign of m.

First, we consider the case of positive m. These columns have no dark state, as shown in Fig. 6. According to the update rule (20), all elements in the mth column can give half of its probability P_m to the right ones and get half of the probability from the left ones by Step I, as shown in Fig. 6. Thus the update rule is given as

$$\begin{aligned}
&\Pi_{M/2}^{(n)} = \Pi_{M/2}^{(n-1)}/2, \\
&\Pi_m^{(n)} = \Pi_m^{(n-1)}/2 + \Pi_{m+1}^{(n-1)}/2 \text{ for } m > 0, \quad m \neq M/2.
\end{aligned} \tag{31}$$

Second, we consider the case for $m \leqslant 0$ where we have $d_{|m|}$ dark states (see Fig. 7). Then, only $({}_M C_{m+\frac{M}{2}} - d_{|m|})$ elements can give the half of its probability P_m to the right ones. Because each element in the mth column have the same

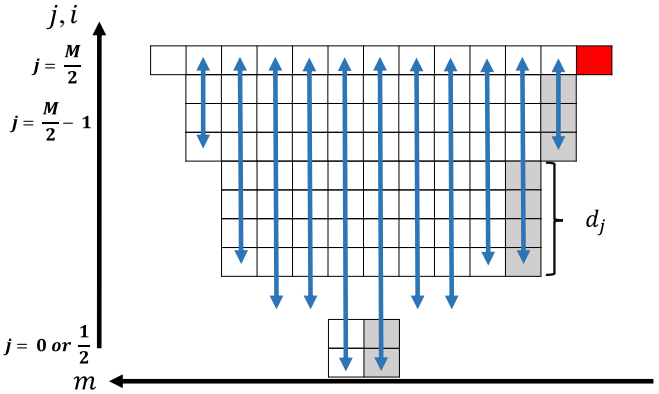

FIG. 4. Global view of the update rule (28) of Step II, which is regarded as averaging of the population of $|j, m, i\rangle$ about j and i for fixed m. The blue arrow in the figure denotes such an averaging.

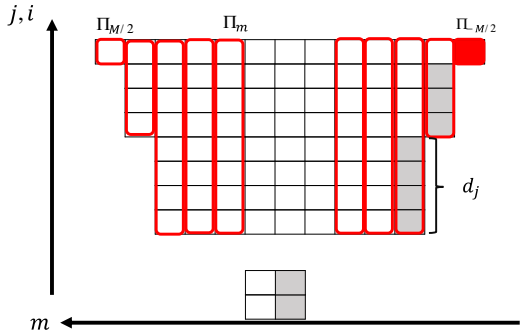

FIG. 5. Definition of Π_m where we sum up all populations of $|j, m, i\rangle$ in the density matrix for a fixed m.

probability P_m due to Step II, we only have to count how many dark states in the mth column in order to derive the update rule. A ratio between the number of the dark states and that of the total elements for a fixed m determines the amount of the population to be transferred from the mth column to the $(m+1)$st column (see Fig. 7). Thus, the update rule for the $m \leqslant 0$ case is given as

$$\Pi_m^{(n)} = \frac{1}{2}\left(1 + \frac{d_{|m|}}{{}_M C_{m+\frac{M}{2}}}\right)\Pi_m^{(n-1)} + \frac{1}{2}\left(1 - \frac{d_{|m+1|}}{{}_M C_{1+m+\frac{M}{2}}}\right)\Pi_{1+m}^{(n-1)}, \quad \text{for } m \leqslant 0, \quad m \neq -M/2,$$

$$\Pi_{-M/2}^{(n)} = \Pi_{-M/2}^{(n-1)} + \frac{1}{2}\left(1 - \frac{d_{|1-M/2|}}{{}_M C_1}\right)\Pi_{1-M/2}^{(n-1)}. \tag{32}$$

The probability of each element $p_{j,m}$ in the mth column can have different values after Step I because the rows labeled by (j, i) are not equivalent. For instance, the probabilities of dark states will be relatively large compared with those of the other states, see Fig. 7. If the probabilities $p_{j,m}$ depend on j, the above update rule does not work because this rule is derived under the assumption that $p_{j,m} = P_m$. Thus, when we repeat only Step I, the variable Π_m is not appropriate to describe our process and we should use the original update rule (20) for $p_{j,m}$. On the other hand, when we insert Step II, since this step averages these probabilities, this update rule for Π_m can be applied for the next repetition of Step I.

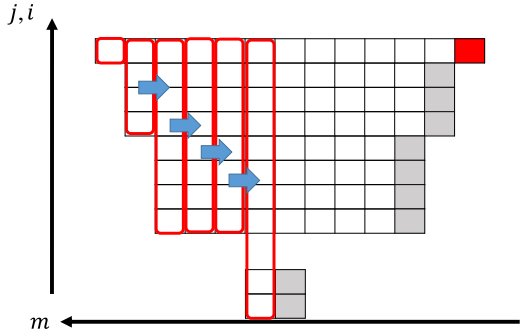

FIG. 6. Update rule for $m > 0$. Half of the population of $|j, m, i\rangle$ is transferred to that of $|j, m-1, i\rangle$.

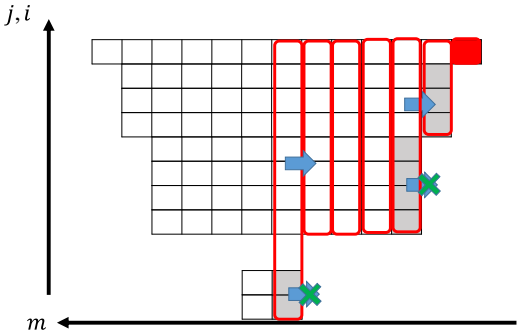

FIG. 7. Update rule for $m \leqslant 0$. Half of the population of $|j, m, i\rangle$ is transferred to that of $|j, m-1, i\rangle$ unless $|j, m, i\rangle$ is a dark state that cannot transfer its population by Step I.

Let us summarize the combined process of Steps I and II. Note that the state after n times repetition is given as

$$\rho^{(n)} = \sum_{m=-M/2}^{M/2} P_m^{(n)} \sum_{j=|m|}^{M/2} \sum_{i=1}^{d_j} |a_{j,m,i}\rangle\langle a_{j,m,i}|, \tag{33}$$

which is justified with the calculation above. By introducing the probability of the mth column after n times repetition like Eq. (29),

$$\Pi_m^{(n)} = \sum_{j=|m|}^{M/2} \sum_{i=1}^{d_j} P_m^{(n)} = {}_M C_{m+\frac{M}{2}} P_m^{(n)},$$

the update rule is summarized as

$$\Pi_{M/2}^{(n+1)} = \Pi_{M/2}^{(n)}/2,$$

$$\Pi_m^{(n+1)} = \Pi_m^{(n)}/2 + \Pi_{m+1}^{(n)}/2, \quad \text{for } m > 0, \quad m \neq M/2,$$

$$\Pi_m^{(n+1)} = \frac{1}{2}\left(1 + \frac{d_{|m|}}{{}_M C_{m+\frac{M}{2}}}\right)\Pi_m^{(n)} + \frac{1}{2}\left(1 - \frac{d_{|m+1|}}{{}_M C_{1+m+\frac{M}{2}}}\right)\Pi_{1+m}^{(n)}, \quad \text{for } m \leqslant 0, \quad m \neq -M/2,$$

$$\Pi_{-M/2}^{(n+1)} = \Pi_{-M/2}^{(n)} + \frac{1}{2}\left(1 - \frac{d_{|1-M/2|}}{{}_M C_1}\right)\Pi_{1-M/2}^{(n)}. \tag{34}$$

As discussed previously, this update rule is based on the fact that $P_m^{(n)}$ is independent of i and j thanks to Step II. By using above $\Pi_m^{(n)}$, the density matrix after n times repetition is given by

$$\rho^{(n)} = \sum_{m=-M/2}^{M/2} \frac{\Pi_m^{(n)}}{{}_M C_{m+\frac{M}{2}}} \sum_{j=|m|}^{M/2} \sum_{i=1}^{d_j} |a_{j,m,i}\rangle\langle a_{j,m,i}|. \tag{35}$$

Let us consider a probability of an excited state of the kth spin,

$$p_{\uparrow,k} = \tfrac{1}{2}\left[1 + \mathrm{Tr}\left(\sigma_z^{(k)}\rho\right)\right]. \tag{36}$$

Note that all spins are now equivalent. In this case, $p_{\uparrow,k}$ has no dependency on k, and thus we drop the index k in this section. The dynamics of $p_\uparrow$ is summarized in Fig. 8 when $M = 10$, 50, 100, and 200. The x axis is the number of steps divided by M. Since we assume that we wait until the system saturates at

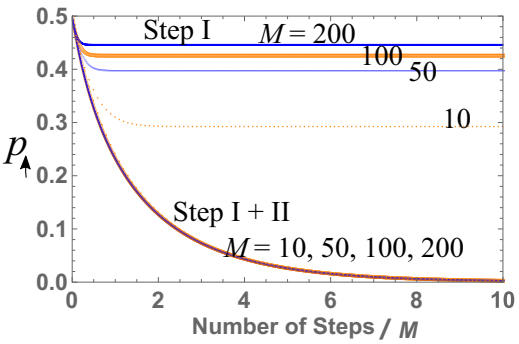

FIG. 8. Plot of the excited-state population $p_\uparrow$ of the spin against the normalized number of steps. When we adopt only Step I, $p_\uparrow$ converges to finite nonzero values. On the other hand, when we adopt Steps I and II, $p_\uparrow$ approaches zero, and the plots behave same regardless of the number of spins. Here, we take $M = 10$, 50, 100, and 200 from the bottom to top where M denotes the number of spins.

each Step I and Step II, the plot is independent of the interaction strength g in Eq. (6) and the dephasing rate of the spins γ' in Eq. (9). When we perform only Step I, the population will be trapped by the dark states, and the final population of the excited state of the spins increases as M does. On the other hand, the excited-state population converges to zero when we perform both Steps I and II, as expected. Also, the plot of Step I + II shows a universal dynamics and does not depend on M.

III. SPIN POLARIZATION WITH A FLUX QUBIT

We analyze a realistic polarization dynamics of electron spins based on the discussion in Sec. II and show numerical simulations in various conditions.

A. Parameters

We simulate the polarization dynamics with realistic parameters according to the Hamiltonian (1) and Lindbladian (2). The configuration of the FQ is assumed to be a $2r_0 \times 2r_0$ square (see Fig. 9) and the parameters for numerical simulations are summarized in Table I.

The electron spins are located in the middle of a square determined by the FQ (see Fig. 9). Their interaction strengths

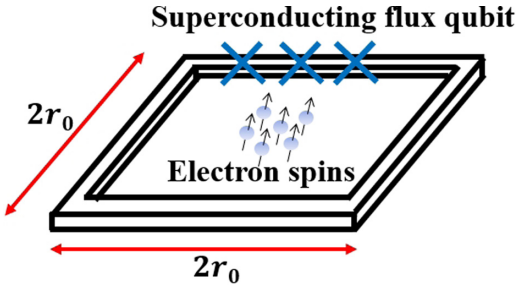

FIG. 9. Illustration of our system composed of the superconducting flux qubit (FQ) and electron spins. The FQ consists in a square loop containing three Josephson junctions, illustrated as three blue ×. The electron spins are located in the middle of the FQ, and they are inductively coupled with the FQ.

TABLE I. Parameters of the FQ for numerical simulations [23,42,43].

Parameter of FQ	Symbol	Value
Size	r_0	$3.0 \times 10\ \mu$m
Persistent current	I_p	180 nA
Longitudinal relaxation time	$T_1^{(\mathrm{FQ})}$	20 μs
Transversal relaxation time	$T_2^{(\mathrm{FQ})}$	2 μs
Energy gap	$\Delta/2\pi$	5.37 GHz
Detuning parameter	$\varepsilon/2\pi$	0.112 GHz
Time required for initialization	t_i	1 μs
Interval between initialization	t_int	4 μs

g_k with the FQ during the spin lock are given as [32,37,38]

$$g_k = \frac{\varepsilon}{\sqrt{\varepsilon^2+\Delta^2}} \frac{\gamma_e \mu_0 I_p}{2\pi} \sum_{i=1}^{4} \frac{1}{r_i^{(k)}}, \tag{37}$$

where $r_i^{(k)}$, γ_e, μ_0 are the distance from ith side of the FQ to a kth spin, the gyromagnetic ratio of an electron spin, and the vacuum permeability, respectively. If the electron spin is placed in the middle of a FQ, we obtain $g_k = g_0 = 175$ rad/s with the parameters given in Table I. This value gives the energy scale of the interaction between the FQ and spins.

In our proposal, a fast FQ initialization is essential. A fast reset in 120 ns was demonstrated with a superconducting transmon qubit [39]. Although the transmon qubit was used, we could in principle use the superconducting flux qubit with a similar setup. We also point out that theoretical proposal for fast initialization of a FQ have been reported [40]. Moreover, there was an experimental demonstration to reset the FQ within tens of nanoseconds by using quantum feedback control [41]. It is worth mentioning that we choose realistic parameters of the coherence time of the FQ for our numerical simulations.

We also assume that the longitudinal relaxation time $T_1^{(e)} = 3600$ s [20] and the transversal relaxation time $T_2^{(e)} = 1.0 \times 10^{-3}$ s for electron spins [16,17,20,44–47].

In Appendix B, we also consider the case in the condition of $T_1^{(\mathrm{FQ})} = 200\ \mu$s, $T_2^{(\mathrm{FQ})} = 30\ \mu$s, and $T_1^{(e)} = 100$ s, which will be realized in the near future. Appendixes C and D discuss how the change of several parameters affect the cooling behavior.

B. Simulations

We numerically calculate the system dynamics according to the operator sum formalism [48–50]. The density matrix ρ is updated as follows:

$$\rho(t) \to \rho' = e^{-i\mathcal{H}\delta}\rho\, e^{i\mathcal{H}\delta} \to \rho(t+\delta) = \rho' + \mathcal{L}[\rho']\delta. \tag{38}$$

Here, we take $\delta = 1\ \mu$s, which is much shorter than the characteristic timescale such as T_1 of the FQ, T_1 and T_2 of the spins, and $1/g_k$. Also, δ is set to be shorter than T_2 of the FQ. The choice of these parameters should not significantly affect the dynamics of our system. We let the system evolve by this formalism for a time t_int. We consider various $\mathcal{H}$ and $\mathcal{L}$ by changing parameters in Secs. III B 1–III B 4.

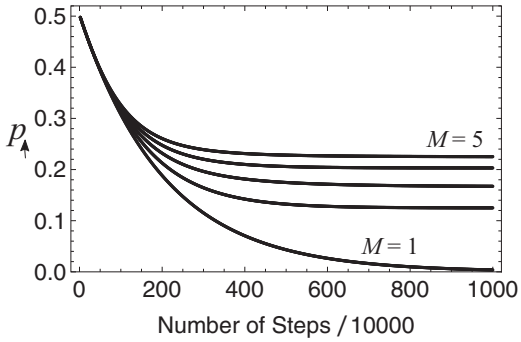

FIG. 10. Plot of the excited-state population $p_\uparrow$ of the spins against the number of steps for $M = 1$–5 of electron spins. The initial state of the spins is a completely mixed state. We set the parameters as $\omega'_{k=1-M} = 0$, $g_{k=1-M} = g_0$, and $\gamma_{\mathrm{T}}^{(\mathrm{l=0-M})} = \gamma_{\mathrm{L}}^{(\mathrm{l=0-M})} = 0$.

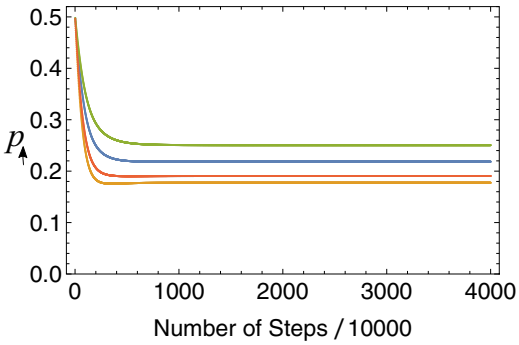

FIG. 11. Plot of the excited-state population $p_{\uparrow,k}$ of the spins against the number of steps for $M = 4$ when $\omega'_{k=1-M} = 0$, $\{g_{k=1-M}\} = \{161, 188, 218, 238\}$ rad/s, $\gamma_{\mathrm{T}}^{(\mathrm{l=0-M})} = \gamma_{\mathrm{L}}^{(\mathrm{l=0-M})} = 0$. The lines from top to bottom correspond to $k = 1$, 2, 3 and 4, respectively.

The initial state of the electron spin is a completely mixed state. We assume that the FQ is periodically initialized into the ground state at $t_n = (n-1)(t_{\mathrm{i}} + t_{\mathrm{int}})$ where n denotes natural numbers. We define this period as a single step. Since the initialization of the FQ can be much faster than the timescale of the decay of the electron spins, we assume that the state of the electron spins does not change during the initialization of the FQ.

In the numerical calculations, we do not separate the dynamics into Step I and Step II. By applying both the dephasing of the electron spins and the interaction between the FQ and the electron spins, we simultaneously perform Step I and Step II.

1. $\omega'_k = 0$, $g_k = g_0$, and $\gamma_{\mathrm{T}}^{(\mathrm{l})} = \gamma_{\mathrm{L}}^{(\mathrm{l})} = 0$ case

We first simulate the case when there is no decoherence in order to illustrate the influence of dark states on the polarization process. We assume that $\omega_k{}' = 0$ and $g_{k=1\sim M} = g_0$ in Eq. (1) and $\gamma_{\mathrm{T}}^{(\mathrm{l=0-M})} = \gamma_{\mathrm{L}}^{(\mathrm{l=0-M})} = 0$ in Eq. (2). Figure 10 shows the dynamics of $p_\uparrow$. Note that all spins are equivalent and thus all $p_{\uparrow,k}$ are identical. Because of the dark states, $p_\uparrow$ saturates in the large-step limit. Note also that the cooling rate in this simulation is much slower than that shown in Fig. 8. This is because the interaction time t_{int} in Fig. 10 is much smaller than $1/g_k$, and the population transfer between the electron spins and the FQ is small at a single step. On the other hand, in Fig. 8, half of the ground-state population is transferred to the electron spins at a single step.

2. $\omega'_k = 0$ and $\gamma_{\mathrm{T}}^{(\mathrm{l})} = \gamma_{\mathrm{L}}^{(\mathrm{l})} = 0$ case

We consider the case when g_k is inhomogeneous because of random spin positioning on a substrate according to Eq. (37).

Figure 11 shows $p_{\uparrow,k}$ when $M = 4$. Due to the different values of g_k (see the caption of Fig. 11), $p_{\uparrow,k}$ approaches a different saturation value and does not approach zero because of dark states as in Fig. 10. Note that there is no direct interaction among spins and the interaction between the FQ and the spins are small. Therefore, the cooling behavior of the spins in the case of larger M is essentially the same as shown in Fig. 11.

3. $\omega'_k = 0$, $\gamma_{\mathrm{T}}^{(\mathrm{l})} \neq 0$, and $\gamma_{\mathrm{L}}^{(\mathrm{l})} = 0$ case

We consider the case when g_k is inhomogeneous with a finite dephasing rate of $\gamma_{\mathrm{T}}^{(\mathrm{l=0-M})} \neq 0$. Figure 12 shows the case with $M = 4$. Due to the dephasing on spins, $p_{\uparrow,k}$ approaches zero with different cooling rate according to g_k. This observation with Fig. 11 shows that the dephasing leads $p_{\uparrow,k} = 0$ at the large-step limit.

4. Realistic case

To support our simplified model discussed in Sec. II, we have considered nonrealistic cases in Sec. III B 1–3 where some imperfections have been ignored. We will, here, discuss a realistic case when both ω'_k and g_k are inhomogeneous with finite decay rates of $\gamma_{\mathrm{T}}^{(\mathrm{l})} \neq 0$ and $\gamma_{\mathrm{L}}^{(\mathrm{l})} \neq 0$.

We show the case for $M = 4$ in Fig. 13. $p_{\uparrow,k}$ approaches 0.08 regardless of ω'_k and g_k. It converges to nonzero values because of $\gamma_{\mathrm{L}}^{(l)} \neq 0$. Due to a thermal relaxation process, the state of the electron spins will be a Gibbs state in a natural environment, and its excited-state population is $p_\uparrow = 0.47$ at 1 mT and 10 mK (a typical operation temperature of a FQ) environment. This means that our cooling scheme with the FQ is especially useful when we perform an ESR with the FQ: A sensitivity of ESR measurements is proportional to $p_\downarrow - p_\uparrow$

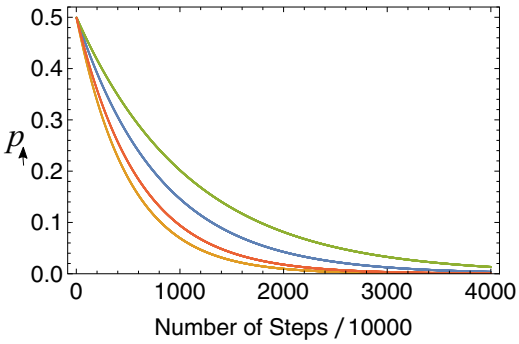

FIG. 12. Plot of the excited-state population, $p_{\uparrow,k}$, of the electron spins against the number of steps for $M = 4$ when $\omega'_{k=1-M} = 0$, $\{g_{k=1-M}\} = \{161, 188, 218, 238\}$ rad/s, $\gamma_{\mathrm{L}}^{(\mathrm{l=0-M})} = 0$, $\gamma_{\mathrm{T}}^{(0)} = 1/T_2^{(\mathrm{FQ})}$, and $\gamma_{\mathrm{T}}^{(k=1-M)} = 1/T_2^{(e)}$. The lines from top to bottom correspond to $k = 1$, 2, 3 and 4, respectively.

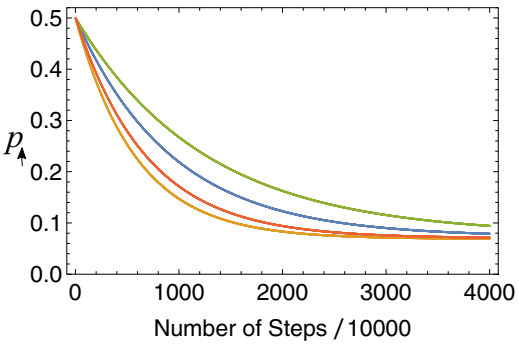

FIG. 13. Realistic simulations. We plot the excited-state population $p_{\uparrow,k}$ of the electron spins against the number of steps for $M = 4$ when $\{g_{k=1-M}\} = \{161, 188, 218, 238\}$ rad/s, $\omega'_{k=1-M}/2 = \{-12487, -7074, 1764, 8946\}$ rad/s, $\gamma_{\rm L}^{(0)} = 1/T_1^{\rm (FQ)}$, $\gamma_{\rm L}^{(k=1-M)} = 1/T_1^{(e)}$, $\gamma_{\rm T}^{(0)} = 1/T_2^{\rm (FQ)}$, and $\gamma_{\rm T}^{(k=1-M)} = 1/T_2^{(e)}$. The lines from top to bottom correspond to $k = 1, 2, 3$ and 4, respectively.

[14,51], and so the sensitivity of ESR with our polarization scheme leads to more than ten times better than the conventional one without active cooling. Also, it is worth mentioning that the actual temperature of the electron spins in the dilution refrigerator might be 50 mK or more and not 10 mK [7,8] because $T_1^{(e)}$ of the electron spins is large [20]. Moreover, an interval between measurements in the standard ESR should be a few time larger than T_1 of the electron spins. Therefore, as $T_1^{(e)}$ becomes longer, our approach becomes more efficient than the conventional approach.

IV. CONCLUSION

In conclusion, we propose a scheme to polarize electron spins with a superconducting flux qubit (FQ). Since we cannot apply large magnetic fields for the FQ to work, there is a large energy gap between the electron spins and FQ. To achieve a strong interaction between them, we adopt a spin-lock technique for the FQ. A Rabi frequency of the FQ can be as small as resonance frequencies of the electron spins and thus the efficient energy transfer between them can occur. We find that homogeneous electron spins without any decoherence cannot be cooled down to the ground state with the FQ, because the electron spins in dark states cannot be coupled to the FQ. Interestingly, dephasing on the electron spins (usually they are not avoidable in experiments) allows them to escape from the dark states. We show that the electron spins can be polarized in realistic conditions by using our scheme.

ACKNOWLEDGMENTS

This work was supported by Leading Initiative for Excellent Young Researchers MEXT Japan, JST presto (JPMJPR1919) Japan, JSPS Grants-in-Aid for Scientific Research (21K03423), and CREST (JPMJCR1774).

APPENDIX A: PROOF OF EQ. (25)

We first prove

$$P\rho_{j,m}P^\dagger = \rho_{j,m} \tag{A1}$$

for any permutation matrix P. Note that any permutation matrix P satisfies

$$[P, S_z] = 0, \quad [P, S^2] = 0, \tag{A2}$$

where $S^2 = S_x^2 + S_y^2 + S_z^2$. This is directly proved by the permutation invariance $PS_zP^\dagger = S_z$ and $PS^2P^\dagger = S^2$ in the following way:

$$\begin{aligned} PS_z &= PS_zP^\dagger P = S_zP, \\ PS^2 &= PS^2P^\dagger P = S^2P, \end{aligned} \tag{A3}$$

where we use $P^{-1} = P^\dagger$.

Let us write the action of P on $|j, m, i\rangle$ as

$$P|j, m, i\rangle = \sum_{j',m',i'} P^{j,m,i}_{j',m',i'}|j', m', i'\rangle. \tag{A4}$$

We consider the explicit form of $P^{j,m,i}_{j',m',i'}$. By considering the following fact:

$$\begin{aligned} 0 &= [P, S_z]|j, m, i\rangle = PS_z|j, m, i\rangle - S_zP|j, m, i\rangle \\ &= mP|j, m, i\rangle - S_z \sum_{j',m',i'} P^{j,m,i}_{j',m',i'}|j', m', i'\rangle \\ &= mP|j, m, i\rangle - \sum_{j',m',i'} m' P^{j,m,i}_{j',m',i'}|j', m', i'\rangle \\ &= \sum_{j',m',i'} (m - m')P^{j,m,i}_{j',m',i'}|j', m', i'\rangle. \end{aligned} \tag{A5}$$

This implies that $P^{j,m,i}_{j',m',i'}$ has the form of $\delta^m_{m'}\tilde{P}^{j,i}_{j',i'}$. By using the commutation relation about S^2, we can prove that $P^{j,m,i}_{j',m',i'}$ has the form of $\delta^m_{m'}\delta^j_{j'}\tilde{P}^i_{i'}$ in the same manner as above. Thus, P is a block-diagonal matrix with respect to the basis $\{|j, m, i\rangle\}_{j,m,i}$. The explicit form of P is given as

$$P = \sum_{j,m,i,i'} \tilde{\tilde{P}}^i_{i'}|j, m, i\rangle\langle j, m, i'| \tag{A6}$$

because P is a unitary matrix. $\tilde{\tilde{P}}^{i'}_i$ is also unitary, i.e., $\sum_{i''} \tilde{\tilde{P}}^i_{i''}(\tilde{\tilde{P}}^{i'}_{i''})^* = \delta_{i,i'}$. Then we can explicitly show

$$\begin{aligned} P\rho_{j,m}P^\dagger &= \sum_{j_{1,2},m_{1,2},i_{1,2,3,4}} \tilde{\tilde{P}}^{i_1}_{i_2}|j_1, m_1, i_1\rangle\langle j_1, m_1, i_2| \\ &\quad \rho_{j,m}\left(\tilde{\tilde{P}}^{i_4}_{i_3}\right)^*|j_2, m_2, i_3\rangle\langle j_2, m_2, i_4| \\ &= \sum_{i,i_1,i_4} \tilde{\tilde{P}}^{i_1}_i \left(\tilde{\tilde{P}}^{i_4}_i\right)^*|j, m, i_1\rangle\langle j, m, i_4| \\ &= \sum_i |j, m, i\rangle\langle j, m, i| = \rho_{j,m}. \end{aligned} \tag{A7}$$

We now proved Eq. (A1), which means that all the diagonal elements of $\rho_{j,m}$ represented in the binary basis ($|\underbrace{11\cdots1}_{n/2+m}\underbrace{00\cdots0}_{n/2-m}\rangle$ and all its permutations) is identical; that

is,

$$\rho_{j,m} = \frac{d_j}{{}_M C_{m+\frac{M}{2}}} |0\rangle\langle 0| \otimes \begin{pmatrix} 1 & . & . & \dots & . \\ . & 1 & . & \dots & . \\ . & . & 1 & \dots & . \\ \vdots & \vdots & \vdots & \ddots & \vdots \\ . & . & . & \dots & 1 \end{pmatrix}. \quad \text{(A8)}$$

This matrix is a ${}_M C_{m+\frac{M}{2}} \times {}_M C_{m+\frac{M}{2}}$ matrix while its matrix rank is d_j. The effect of independent dephasing $\mathcal{E}_{\rm II}$ makes the nondiagonal elements of this matrix be 0. Thus, after Step II, the density matrix $\rho_{j,m}$ becomes $\mathcal{E}_{\rm II}(\rho_{j,m})$ given as

$$\mathcal{E}_{\rm II}(\rho_{j,m}) = \frac{d_j}{{}_M C_{m+\frac{M}{2}}} |0\rangle\langle 0| \otimes \begin{pmatrix} 1 & 0 & 0 & \dots & 0 \\ 0 & 1 & 0 & \dots & 0 \\ 0 & 0 & 1 & \dots & 0 \\ \vdots & \vdots & \vdots & \ddots & \vdots \\ 0 & 0 & 0 & \dots & 1 \end{pmatrix}, \quad \text{(A9)}$$

which is the identity matrix of the space spanned by the binary basis with fixed m. Although the above matrix is represented in the binary basis, because the identity matrix is invariant under any unitary transformation on this space, Eq. (A9) can be rewritten as

$$\mathcal{E}_{\rm II}(\rho_{j,m}) = \frac{d_j}{{}_M C_{m+\frac{M}{2}}} |0\rangle\langle 0| \otimes \sum_{s=|m|}^{M/2} \sum_{i=1}^{d_s} |s, m, i\rangle\langle s, m, i|. \quad \text{(A10)}$$

Thus, Eq. (25) is proved.

APPENDIX B: EXPECTED EXPERIMENTS IN NEAR FUTURE

The coherence time used for the numerical simulation so far is realistic with the current technology. However, since the coherence time of the superconducting qubit are expected to become longer due to the development of the technology, we also performed the simulations in the condition of $T_1^{(\rm FQ)} = 200\ \mu$s, $T_2^{(\rm FQ)} = 30\ \mu$s, $T_1^{(e)} = 100$ s, $t_{\rm i} = 5\ \mu$s, $t_{\rm int} = 95\ \mu$s, and $\delta = 5\ \mu$s.

We show the case for $M = 7$ in Fig. 14 which should be compared with Fig. 13. Because of the longer $T_1^{(\rm FQ)}$ and $T_2^{(\rm FQ)}$, the cooling rate of electron spins is much faster. $p_{\uparrow,k}$ approaches 0.17 regardless of ω'_k and g_k.

APPENDIX C: COOLING BEHAVIOR AS A FUNCTION OF g AND $T_2^{(\rm FQ)}$

From Eq. (16), we can suppose that $\varsigma := g^2 T_2^{(\rm FQ)} t_{\rm int}$ is an important parameter that determines the behavior of cooling. The bottleneck of the speed of cooling in one step is the slower mode $\frac{-\gamma_T^{(0)} + (\gamma_T^{(0)} - 16 g^2 l_{jm}^2)^{1/2}}{2}$. We now use $\gamma_T^{(0)} = 1/T_2^{(\rm FQ)}$ instead of γ in Eq. (16). This eigenvalue can be expanded as $16 g^2 l_{jm}^2 / \gamma_T^{(0)} = 16 g^2 l_{jm}^2 T_2^{(\rm FQ)}$ when $g \ll \gamma_T^{(0)}$. The competition between $1/t_{\rm int}$ and $16 l_{jm}^2 g^2 T_2^{(\rm FQ)}$ determines the behavior of cooling. Thus, we can take ς as a key parameter for the cooling behavior.

Here, we evaluate how the change in ς affects the cooling behavior in numerical calculations. We assume that the spins are homogeneous: $\omega'_k = 0$ and $g_k = g_0$. The other parameters

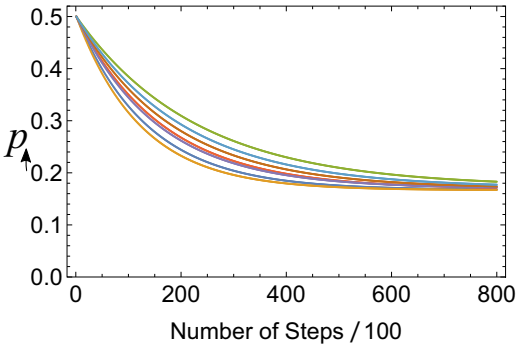

FIG. 14. Realistic simulations. We plot the excited-state population $p_{\uparrow,k}$ of the electron spins against the number of steps for $M = 7$ when $\omega'_{k=1-M}/2 = \{-3459, -911, -3511, 4082, 12114, 4608, -6898\}$ rad/s, $\{g_{k=1-M}\} = \{150, 160, 169, 178, 190, 197, 209\}$ rad/s, $\gamma_{\rm L}^{(0)} = 1/(200\ \mu$s), $\gamma_{\rm L}^{(k=1-M)} = 1/(100$ s), $\gamma_{\rm T}^{(0)} = 1/(30\ \mu$s), and $\gamma_{\rm T}^{(k=1-M)} = 1/(1$ ms). The lines from top to bottom correspond to $k = 1, 2, 3, 4, 5, 6$ and 7, respectively.

are set to be $\gamma_T^{(k)} = 1/(1$ ms), $\gamma_L^{(0)} = 1/(200\ \mu$s), $t_{\rm i} = 5\ \mu$s, $t_{\rm int} = 95\ \mu$s, $\delta = 5\ \mu$s, which are same as in Appendix B, and $\gamma_L^{(k)} = 0$. Also, we consider the $M = 2$ case for simplicity.

First, we calculate the cooling speed at early steps for several pairs of $(g_0, T_2^{(\rm FQ)})$. We approximate the cooling speed v at early steps by

$$v = \left| \frac{(p_\uparrow \text{ at the 2000th step}) - (p_\uparrow \text{ at the initial time})}{2000} \right|.$$

Figure 15 plots the cooling speed v as a function of ς. These points are almost on the same curve for small ς. This result is consistent with our claim that ς is an important parameter for the cooling behavior.

We also evaluate the entire dynamics while changing ς. Figure 16 plots the dynamics for several values of ς while we took $\varsigma \approx 8.7 \times 10^{-5}$ as in Appendix B. However, this result shows that the state of the spin ensemble approaches to almost the same stationary state even when ς changes by several orders of magnitude. On the other hand, the cooling speed significantly changes depending on ς.

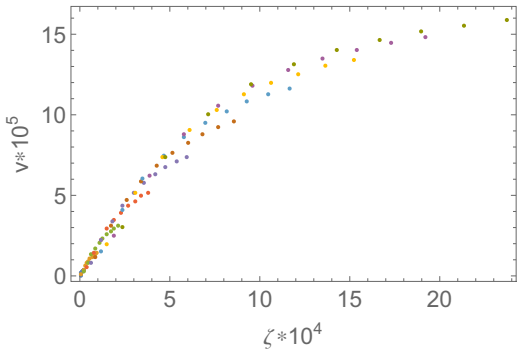

FIG. 15. Cooling speed at early steps v as a function of ς. We plot v for any pair of $g_0 = \{50, 100, 150, 200, 250, 300, 350, 400, 450, 500\}$ rad/s and $T_2^{(\rm FQ)} = \{10, 20, 30, 40, 50, 60, 70, 80, 90, 100\}\ \mu$s. Regardless of the combinations of g_0 and $T_2^{(\rm FQ)}$, v, is universal as a function of ς.

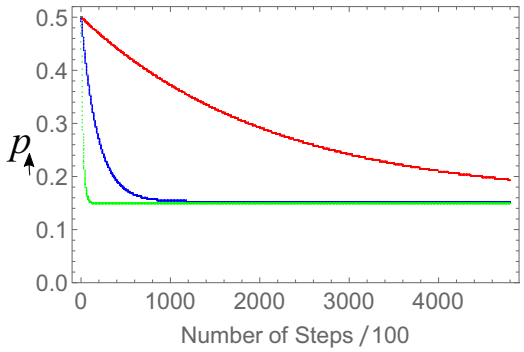

FIG. 16. The behavior of cooling for three values of ς. The lines from top to the bottom correspond to $\varsigma = 0.71 \times 10^5$, 8.6×10^5, and 76×10^5, respectively.

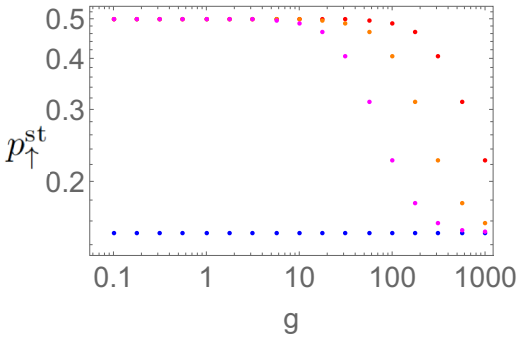

FIG. 17. The excited-state probability $p_\uparrow^{\rm st}$ at the stationary state as a function of g. The lines from top to bottom correspond to $T_1^{(e)} =$ 1 s, 10 s, 100 s, and ∞, respectively.

APPENDIX D: STATIONARY STATE IN FINITE-T_1 CASES

Here we consider whether quantum spin systems with small g can be polarized or not. In Fig. 17, we plot the excited-state probability $p_\uparrow^{\rm st}$ at the stationary state. We consider the $M = 1$ case in this Appendix and the parameters other than $T_1^{(e)}$ are the same as in the Appendix B.

For $T_1^{(e)} = \infty$, $p_\uparrow^{st}$ is almost independent of g as also implied in Appendix C. On the other hand, the g dependence of $p_\uparrow^{\rm st}$ appears once we take the effect of $T_1^{(e)}$ into account. For $T_1^{(e)} = 100$ s that we use in Appendix B, we need a coupling strength of $g \sim O(10^2)$ to obtain the maximum polarization. If we try to polarize spins with $g \approx 0.1$ rad/s, we will need a much longer $T_1^{(e)}$.

[1] Y. Kubo, I. Diniz, C. Grezes, T. Umeda, J. Isoya, H. Sumiya, T. Yamamoto, H. Abe, S. Onoda, T. Ohshima, V. Jacques, A. Dreau, J. F. Roch, A. Auffeves, D. Vion, D. Esteve, and P. Bertet, Phys. Rev. B **86**, 064514 (2012).

[2] H. Toida, Y. Matsuzaki, K. Kakuyanagi, X. Zhu, W. J. Munro, K. Nemoto, H. Yamaguchi, and S. Saito, Appl. Phys. Lett. **108**, 052601 (2016).

[3] A. Bienfait, J. Pla, Y. Kubo, M. Stern, X. Zhou, C. Lo, C. Weis, T. Schenkel, M. Thewalt, D. Vion *et al.*, Nat. Nanotechnol. **11**, 253 (2016).

[4] C. Eichler, A. J. Sigillito, S. A. Lyon, and J. R. Petta, Phys. Rev. Lett. **118**, 037701 (2017).

[5] S. Probst, A. Bienfait, P. Campagne-Ibarcq, J. Pla, B. Albanese, J. Da Silva Barbosa, T. Schenkel, D. Vion, D. Esteve, K. Mølmer *et al.*, Appl. Phys. Lett. **111**, 202604 (2017).

[6] A. Bienfait, P. Campagne-Ibarcq, A. H. Kiilerich, X. Zhou, S. Probst, J. J. Pla, T. Schenkel, D. Vion, D. Esteve, J. J. L. Morton, K. Moelmer, P. Bertet *et al.*, Phys. Rev. X **7**, 041011 (2017).

[7] R. P. Budoyo, K. Kakuyanagi, H. Toida, Y. Matsuzaki, W. J. Munro, H. Yamaguchi, and S. Saito, Phys. Rev. Mater. **2**, 011403(R) (2018).

[8] H. Toida, Y. Matsuzaki, K. Kakuyanagi, X. Zhu, W. J. Munro, H. Yamaguchi, and S. Saito, Commun. Phys. **2**, 33 (2019).

[9] V. Ranjan, S. Probst, B. Albanese, T. Schenkel, D. Vion, D. Esteve, J. Morton, and P. Bertet, Appl. Phys. Lett. **116**, 184002 (2020).

[10] Y. Wiemann, J. Simmendinger, C. Clauss, L. Bogani, D. Bothner, D. Koelle, R. Kleiner, M. Dressel, and M. Scheffler, Appl. Phys. Lett. **106**, 193505 (2015).

[11] Y.-H. Chen, X. Fernandez-Gonzalvo, S. P. Horvath, J. V. Rakonjac, and J. J. Longdell, Phys. Rev. B **97**, 024419 (2018).

[12] G. Yue, L. Chen, J. Barreda, V. Bevara, L. Hu, L. Wu, Z. Wang, P. Andrei, S. Bertaina, and I. Chiorescu, Appl. Phys. Lett. **111**, 202601 (2017).

[13] R. P. Budoyo, K. Kakuyanagi, H. Toida, Y. Matsuzaki, and S. Saito, Appl. Phys. Lett. **116**, 194001 (2020).

[14] J. Wertz, *Electron Spin Resonance: Elementary Theory and Practical Applications* (Springer Science & Business Media, Berlin, 2012).

[15] E. M. Purcell, in *Confined Electrons and Photons* (Springer, Berlin, 1995), pp. 839.

[16] A. Bienfait, J. Pla, Y. Kubo, X. Zhou, M. Stern, C. Lo, C. Weis, T. Schenkel, D. Vion, D. Esteve *et al.*, Nature (London) **531**, 74 (2016).

[17] R. Amsüss, C. Koller, T. Nöbauer, S. Putz, S. Rotter, K. Sandner, S. Schneider, M. Schramböck, G. Steinhauser, H. Ritsch, J. Schmiedmayer, and J. Majer, Phys. Rev. Lett. **107**, 060502 (2011).

[18] S. Probst, H. Rotzinger, S. Wünsch, P. Jung, M. Jerger, M. Siegel, A. V. Ustinov, and P. A. Bushev, Phys. Rev. Lett. **110**, 157001 (2013).

[19] A. Angerer, S. Putz, D. O. Krimer, T. Astner, M. Zens, R. Glattauer, K. Streltsov, W. J. Munro, K. Nemoto, S. Rotter, J. Schmiedmayer, and J. Majer, Sci. Adv. **3**, e1701626 (2017).

[20] R. P. Budoyo, K. Kakuyanagi, H. Toida, Y. Matsuzaki, W. J. Munro, H. Yamaguchi, and S. Saito, Appl. Phys. Express **11**, 043002 (2018).

[21] S. Hartmann and E. Hahn, Phys. Rev. **128**, 2042 (1962).

[22] J. Q. You, X. Hu, S. Ashhab, and F. Nori, Phys. Rev. B **75**, 140515(R) (2007).

[23] F. Yan, S. Gustavsson, A. Kamal, J. Birenbaum, A. P. Sears, D. Hover, T. J. Gudmundsen, D. Rosenberg, G. Samach, S. Weber *et al.*, Nat. Commun. **7**, 12964 (2016).

[24] L. V. Abdurakhimov, I. Mahboob, H. Toida, K. Kakuyanagi, and S. Saito, Appl. Phys. Lett. **115**, 262601 (2019).
[25] A. Laraoui and C. A. Meriles, ACS Nano **7**, 3403 (2013).
[26] J. Scheuer, I. Schwartz, Q. Chen, D. Schulze-Sünninghausen, P. Carl, P. Höfer, A. Retzker, H. Sumiya, J. Isoya, B. Luy *et al.*, New J. Phys. **18**, 013040 (2016).
[27] F. Yoshihara, Y. Nakamura, F. Yan, S. Gustavsson, J. Bylander, W. D. Oliver, and J. S. Tsai, Phys. Rev. B **89**, 020503(R) (2014).
[28] J. Ping, F. Wang, and J.-q. Chen, *Group Representation Theory for Physicists* (World Scientific Publishing Company, Singapore, 2002).
[29] K.-J. Boller, A. Imamoğlu, and S. E. Harris, Phys. Rev. Lett. **66**, 2593 (1991).
[30] M. Fleischhauer, A. Imamoglu, and J. P. Marangos, Rev. Mod. Phys. **77**, 633 (2005).
[31] X. Zhu, Y. Matsuzaki, R. Amsüss, K. Kakuyanagi, T. Shimo-Oka, N. Mizuochi, K. Nemoto, K. Semba, W. J. Munro, and S. Saito, Nat. Commun. **5**, 3524 (2014).
[32] Y. Matsuzaki, X. Zhu, K. Kakuyanagi, H. Toida, T. Shimo-Oka, N. Mizuochi, K. Nemoto, K. Semba, W. J. Munro, H. Yamaguchi, and S. Saito, Phys. Rev. Lett. **114**, 120501 (2015).
[33] Y. Matsuzaki, X. Zhu, K. Kakuyanagi, H. Toida, T. Shimooka, N. Mizuochi, K. Nemoto, K. Semba, W. J. Munro, H. Yamaguchi, S. Saito *et al.*, Phys. Rev. A **91**, 042329 (2015).
[34] S. Putz, A. Angerer, D. O. Krimer, R. Glattauer, W. J. Munro, S. Rotter, J. Schmiedmayer, and J. Majer, Nat. Photonics **11**, 36 (2017).
[35] B. Julsgaard, C. Grezes, P. Bertet, and K. Mølmer, Phys. Rev. Lett. **110**, 250503 (2013).
[36] S. Probst, H. Rotzinger, A. V. Ustinov, and P. A. Bushev, Phys. Rev. B **92**, 014421 (2015).
[37] D. Marcos, M. Wubs, J. M. Taylor, R. Aguado, M. D. Lukin, and A. S. Sørensen, Phys. Rev. Lett. **105**, 210501 (2010).
[38] J. Twamley and S. D. Barrett, Phys. Rev. B **81**, 241202(R) (2010).
[39] M. D. Reed, B. R. Johnson, A. A. Houck, L. DiCarlo, J. M. Chow, D. I. Schuster, L. Frunzio, and R. J. Schoelkopf, Appl. Phys. Lett. **96**, 203110 (2010).
[40] H. Hsu, M. Silveri, A. Gunyhó, J. Goetz, G. Catelani, and M. Möttönen, Phys. Rev. B **101**, 235422 (2020).
[41] K. Kakuyanagi, A. Kemp, T. Baba, Y. Matsuzaki, H. Nakano, K. Semba, and S. Saito, arXiv:1509.00580.
[42] J. Bylander, S. Gustavsson, F. Yan, F. Yoshihara, K. Harrabi, G. Fitch, D. G. Cory, Y. Nakamura, J. S. Tsai, and W. D. Oliver, Nat. Phys. **7**, 565 (2011).
[43] M. Stern, G. Catelani, Y. Kubo, C. Grezes, A. Bienfait, D. Vion, D. Esteve, and P. Bertet, Phys. Rev. Lett. **113**, 123601 (2014).
[44] A. M. Tyryshkin, S. Tojo, J. J. Morton, H. Riemann, N. V. Abrosimov, P. Becker, H.-J. Pohl, T. Schenkel, M. L. Thewalt, K. M. Itoh *et al.*, Nat. Mater. **11**, 143 (2012).
[45] E. Herbschleb, H. Kato, Y. Maruyama, T. Danjo, T. Makino, S. Yamasaki, I. Ohki, K. Hayashi, H. Morishita, M. Fujiwara *et al.*, Nat. Commun. **10**, 3766 (2019).
[46] A. Jarmola, V. M. Acosta, K. Jensen, S. Chemerisov, and D. Budker, Phys. Rev. Lett. **108**, 197601 (2012).
[47] T. Astner, J. Gugler, A. Angerer, S. Wald, S. Putz, N. J. Mauser, M. Trupke, H. Sumiya, S. Onoda, J. Isoya *et al.*, Nat. Mater. **17**, 313 (2018).
[48] P. Zanardi, Phys. Rev. A **57**, 3276 (1998).
[49] Y. Kondo, Y. Matsuzaki, K. Matsushima, and J. G. Filgueiras, New J. Phys. **18**, 013033 (2016).
[50] M. Bando, T. Ichikawa, Y. Kondo, N. Nemoto, M. Nakahara, and Y. Shikano, Sci. Rep. **10**, 2126 (2020).
[51] K. Miyanishi, Y. Matsuzaki, H. Toida, K. Kakuyanagi, M. Negoro, M. Kitagawa, and S. Saito, Phys. Rev. A **101**, 052303 (2020).